THEORY, MEASUREMENTS, AND MODELS OF THE UPPER ATMOSPHERE AND IONOSPHERE OF SATURN

S. K. ATREYA
The University of Michigan

J. H. WAITE, JR.
Marshall Space Flight Center

T. M. DONAHUE and A. F. NAGY
The University of Michigan

J. C. McCONNELL
York University

The structure and composition of the thermosphere, exosphere and ionosphere of Saturn have been determined from observations at optical and radio wavelengths, principally by instruments aboard Voyager spacecraft. Interpretation of these observations yields an average neutral temperature of 140 K in the stratosphere and mesosphere, a thermospheric temperature gradient of ~ 1.25 K km^{-1}, and an exospheric temperature between 600 K and 800 K for the equatorial region. The amount of power deposited in auroral bands is ~ 2 × 10^{11} W, which is insufficient for the thermospheric heating observed in nonauroral regions. Joule heating and energy deposition from inertia-gravity waves are important candidates as sources of the relatively high exospheric temperature on Saturn. A methane mixing ratio of 1.4 × 10^{-4} measured 965 km above the 1-bar level is indicative of the depletion of this species in the upper atmosphere due to photolysis and diffusion. The strength of vertical mixing is deduced from an analysis of the atomic hydrogen and helium Lyman-α airglow, and from a study of the photochemistry of methane. The value of the eddy mixing coefficient at the homopause is found to be on the order of 10^{8} cm^{2} s^{-1}; the corresponding pressure is a few nanobars. A model of the ionosphere is developed and com-

pared with the results of radio occultation measurements. There is a discrepancy in the altitude and the magnitude of the peak electron concentration. Of several possibilities discussed, the loss of topside protons, reacting with vibrationally excited molecular hydrogen, along with vertical ion drifts, are the most plausible explanations of the discrepancy. It should be emphasized, however, that a meaningful comparison between models and the measured ionospheric profiles will be possible only after data for the lower ionosphere (below ~ 2000 km) have been analyzed. Although there are many apparent similarities between the aeronomy of Saturn and Jupiter, there are distinct differences in terms of the quantitative behavior of the dynamics, energy budget and the plasma processes.

Groundbased spectroscopic measurements in the visible, infrared and microwave during the past two decades and prior to the Voyager observations provided some information on the bulk composition of the Saturn atmosphere. A summary of these measurements is presented in Table I. The Voyager infrared observations (Hanel et al. 1981*a*) have yielded extensive data on

TABLE I
Pre-Voyager Composition Measurements of the Saturn Atmosphere

Species	Spectral Region	References
H_2	S(0) & S(1) quadrupole lines of the (4,0) & (3,0) rotational-vibrational system	Münch and Spinrad (1963); Giver and Spinrad (1966); Owen (1969); Encrenaz and Owen (1973).
CH_4	$3\nu_3$ band in the 1.1 μm region	Trafton (1973); Trafton and Macy (1975); Lecacheux et al. (1976); Combes et al. (1977).
$^{13}CH_4$	1.1 μm	Combes et al. (1977).
C_2H_6	ν_9 at 12.2 μm	Gillett and Forrest (1974); Tokunaga et al. (1975).
PH_3	10–11 μm 5 μm	Encrenaz et al. (1975). Fink and Larson (1977).
CH_3D	5 μm	Fink and Larson (1977).
HD	$P_4(1)$ at 0.7467 μm $R_5(0)$	Trauger et al. (1977). Smith and Macy (1977).
NH_3	0.6450 μm 1.56 μm Radio	Woodman et al. (1977). Owen et al. (1977). Gulkis et al. (1969); Gulkis and Poynter (1972).
H_2S	1.59 μm 0.21–0.25 μm	Owen et al. (1977): upper limit. Caldwell (1977*b*): upper limit.
H	0.1216 μm	Weiser et al. (1977); Barker et al. (1980); Clarke et al. (1981).

the spatial and temporal variations of the above-mentioned species and many more. The first *in situ* measurements of the temperature structure of the upper atmosphere and the distribution of neutral species were provided by the Voyager ultraviolet spectrometer which monitored the sunlight scattered from Saturn's atmosphere, and also sunlight and starlight absorbed by atmospheric species. Complementary information on the structure and composition of the upper atmosphere was provided by the Voyager infrared and radio science investigations. Section I is devoted to the discussion of the neutral upper atmosphere.

The physics and chemistry of the neutral atmosphere and the ionosphere of Saturn are strongly coupled. Although the presence of an extensive ionosphere on Saturn was predicted by several theoretical models, measurements were possible only from the Pioneer and Voyager spacecraft by radio occultation. The first confirmation and measurement of a magnetic field on Saturn was made by the Pioneer vector helium and fluxgate magnetometers (E. J. Smith et al. 1980; Acuna and Ness 1980). Section II deals with the ionospheric measurements, modeling, and the coupling with the neutral atmosphere. Some discussions in this chapter are frequently complementary to those in the chapters on the lower atmosphere (see e.g. chapters by Prinn et al. and Ingersoll et al.).

I. UPPER ATMOSPHERE

The atmosphere of Saturn above the ammonia cloud tops may be conveniently divided into three regions: (1) troposphere with pressures $\gtrsim$ 1 mbar; (2) middle atmosphere or the region of "information gap" with pressures between 1 mbar and 10 nbar; and (3) thermosphere and exosphere with pressures $\lesssim$ 10 nbar. The atmosphere is mixed to the homopause having pressures $\approx$ 1 nbar (Sec. I.B). However, photochemical processes cause departure from a mixed atmospheric distribution of certain species, such as NH_3, CH_4 and PH_3. Discussion of the neutral atmosphere in this chapter is limited to processes occurring primarily in the thermosphere and exosphere, although photochemistry in the mesosphere is included when it is important for understanding the aeronomy of the upper atmosphere. We discuss, in the following sections, techniques for the determination of the vertical profiles of temperature and density, and atmospheric vertical mixing.

A. Temperature and Density Distributions in the Upper Atmosphere

There have been no stellar occultations suitable for groundbased studies of the upper atmosphere of Saturn, thus there are no groundbased data to provide vertical profiles of the temperature or density in the upper atmosphere of Saturn. Results obtained from the inversion of the ionospheric radio occultation data (Kliore et al. 1980*a*; Tyler et al. 1981,1982*a*) are dependent on assumptions regarding ion drifts, ionospheric composition and ion-electron en-

ergy loss processes. Therefore, the most direct means for determining neutral upper atmospheric characteristics was provided by the Voyager ultraviolet spectrometer when it monitored the absorption of sunlight or starlight passing through the atmosphere. Supplementary information was obtained from the interpretation of the reflected sunlight measured by the ultraviolet spectrometer during and before the encounter. Measurement techniques and results are discussed below.

1. Stellar and Solar Occultation. The technique of ultraviolet stellar and solar occultations has been used successfully to determine height profiles of ozone, oxygen, chlorine, and molecular hydrogen in the terrestrial atmosphere (Hays and Roble 1973*a*,*b*; Atreya 1981). In this technique, the atmosphere acts as an absorption cell providing a long pathlength to the ultraviolet radiation from a suitable bright source such as the Sun or a star. By monitoring the tangent rays before and after they pass through the "cell," it is possible to determine the distribution (hence scale height) of the absorbing gases.

If I_0 represents unattenuated flux at wavelength λ and I_z is the flux at some tangent altitude z after absorption by a given molecular species, then

$$I_z = I_0 \exp(-\tau) \tag{1}$$

where $\tau = N \sigma_a$, N is the line-of-sight column abundance of the absorbing gas, and σ_a is its absorption cross section at wavelength λ. I_z and I_0 are monitored by the spectrometer; σ_a is measured in the laboratory. The unknown quantity N is thus

$$N = \frac{1}{\sigma_a} \ln (I_0/I_z). \tag{2}$$

One can invert N by Abel inversion, or numerical inversion techniques (Atreya 1981) to yield local number density n of the absorbing gas. Using a set of different wavelengths, one can determine n at different heights in the atmosphere, if the absorption cross sections are different at the different wavelengths selected. The scale height, hence the temperature, can then be determined by using the hydrostatic law,

$$n_2 = n_1 \exp (-\Delta z/H). \tag{3}$$

Δz can be determined by knowing the rate of descent of the minimum tangent altitude in the atmosphere, which in turn is obtained from the spacecraft/satellite velocity data.

The above technique works best in the region of continuum absorption by a single species. In the outer planets, solar occultation experiments thus provide useful information on the H_2 density from the analysis of continuous ab-

sorption in H_2 below ~ 845 Å. In the case of stellar occultations, the flux below 911 Å is negligible due to the interplanetary/interstellar absorption by hydrogen. Thus, the upper atmospheric H_2 density and temperature determinations require unfolding of absorptions in the Lyman and Werner bands of H_2, as discussed later. Band absorptions in the hydrocarbons pose another challenge, that of isolating absorptions by individual species; the details will be discussed below.

Using the Sun and stars as light sources, it is possible to determine the structure of the upper atmosphere of Jupiter (Broadfoot et al. 1979; Sandel et al. 1979; Atreya et al. 1979*a*; Atreya et al. 1981; Festou et al. 1981). Similar techniques were used on both Voyagers 1 and 2 to determine density and temperature profiles of Saturn's upper atmosphere (Broadfoot et al. 1981; Sandel et al. 1982*b*). At the very short wavelengths used, absorption is much more important than refraction, which is responsible for the effects studied in the visible and radio ranges (Hunten and Veverka 1976). The most successful of these experiments was exit occultation of the star δ Scorpii (Dzuba), in which the passage of tangent rays through the atmosphere of Saturn was unaffected by absorption due to the rings of Saturn.

The ultraviolet flux of star δ Sco (type B0) is much greater than that of α Leo which was used in the Voyager/Jupiter occultation experiment (Festou et al. 1981; Atreya et al. 1981). As a consequence, better statistics resulted in the Voyager/Saturn data. We show in Fig. 1 the unattenuated spectrum of δ Sco (Festou and Atreya 1982) recorded by the Voyager 2 ultraviolet spectrometer on the day of the occultation, 25 August 1981. The data have been corrected for the instrumental scattering and fixed pattern noise. The effective wavelength resolution between 500 Å and 1700 Å is 25 Å; the height resolution is 3.2 km. The exit occultation occurred very near the equator, at 3°.8N. The sharp Lyman cutoff below 911 Å in Fig. 1 is an indication of the strong interstellar hydrogen absorption. A decrease in the instrument sensitivity at ~ 1000 Å is reflected by the reduced signal beyond 1060 Å in Fig. 1.

The principal absorbers of the ultraviolet radiation in the upper atmosphere are H_2, CH_4, C_2H_2, and C_2H_6. Absorption of the signal below 1200 Å is due mainly to molecular hydrogen, and above 1200 Å to the hydrocarbons in the upper atmosphere of Saturn. The data in the vicinity of 1216 Å are not usable due to the strong interplanetary/interstellar Lyman-α absorption. Shown in Figs. 2 and 3 are exit occultation data for H_2 and the hydrocarbons, respectively. The lower abscissa in Figs. 2 and 3 represents altitudes above the 1-bar atmospheric pressure level. Δz is the altitude above the 1-bar level where total extinction in the H_2 absorption channels (here, 939–1023 Å) was recorded by the ultraviolet spectrometer. The spacecraft trajectory information appropriate to the geometry of the δ Sco occultation yields a value for the radius of Saturn at the 1-bar level of 60,246 ± 10 km (Festou and Atreya 1982). Radii of the tangent rays measured from the planetary center are indicated on the upper abscissa of Figs. 2 and 3.

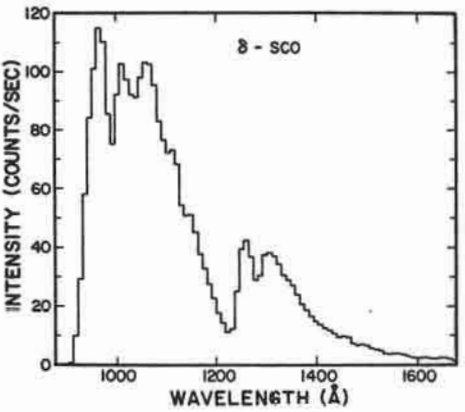

Fig. 1. Unattenuated spectrum of star δ Sco as seen by the Voyager ultraviolet spectrometer. The effective spectral resolution is ~ 25 Å. Background has been removed and the various instrumental corrections applied (after Festou and Atreya 1982).

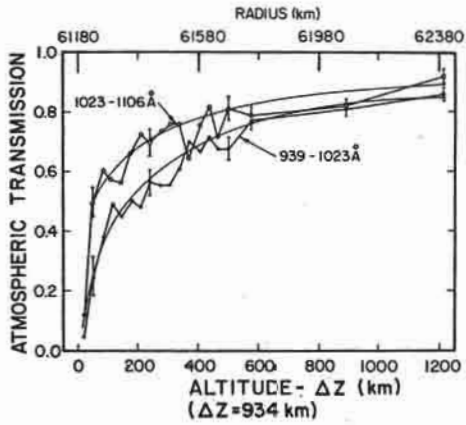

Fig. 2. Absorption by H_2. The lower abscissa shows altitudes above the 1-bar pressure level while the upper abscissa gives corresponding planetocentric radii of the tangent ray points. The height resolution in this figure is 3.2 km, except for points above (Δz + 500) km which have been obtained by averaging 40 consecutive spectra recorded over a 128-km height range. The continuous lines are the absorption curves which are used to derive the temperature and density profiles of H_2 (after Festou and Atreya 1982).

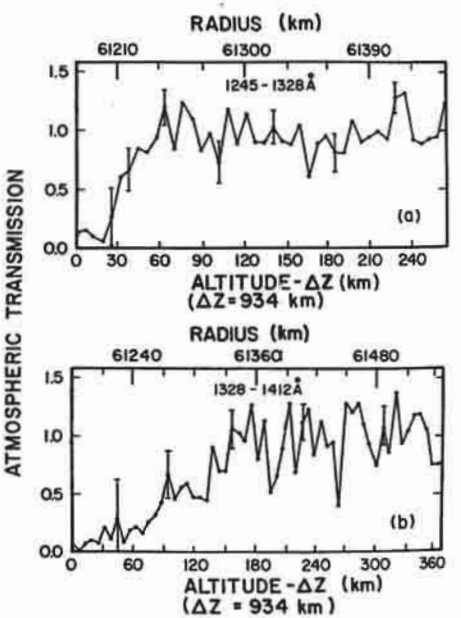

Fig. 3. Absorption by the hydrocarbons. In plot (a) the absorption is attributed to CH_4; in (b), the absorption is due to an unidentified species, alone or in mixture with the hydrocarbons. Altitude scale is the same as in Fig. 2 (after Festou and Atreya 1982).

In the 912–1200 Å range, molecular hydrogen absorbs in the Lyman and Werner bands that connect the ground state $X^1\Sigma_g^+$ with the excited state $B^1\Sigma_g^+$ and $C^1\Pi_u$, respectively. Assuming a Voigt profile (natural and Doppler broadening) for each vibrational-rotational line in the Lyman and Werner band systems, one calculates atmospheric transmission as a function of frequency; the theoretical calculations done by Festou et al. (1981) are shown in Fig. 4. Using simulated transmissions and the lightcurves shown in Fig. 2, Festou and Atreya (1982) have shown that the best fit to the data requires a temperature of 800^{+150}_{-120} K at and beyond 1540 km; the H_2 density at this altitude is found to be $5^{+3.6}_{-1.8} \times 10^9$ cm^{-3}. A temperature gradient of $1.25^{+0.05}_{-0.07}$ K km^{-1} is obtained from approximately 950 to 1540 km.

Absorption shown in the lightcurve for 1245–1328 Å (Fig. 3a) can be explained satisfactorily by methane alone (Festou and Atreya 1982). This assumption is further substantiated by the fact that on examining absorption

characteristics of individual 9 Å wide channels within the wavelength range covered in Fig. 3a, one finds that a given optical depth always occurs at the same altitude. Since absorption cross sections of both C_2H_2 and C_2H_4 have large variation in this wavelength range, they cannot account for the observed transmission characteristics. C_2H_6 is not acceptable either since at shorter wavelengths it produces more than the observed absorption around 985 km. Inversion of the absorption characteristics shown in Fig. 3a facilitates the determination of the CH_4 density in the short altitude interval ranging from approximately 934 km to 994 km. The CH_4 density determination, however, is most accurate in the middle of this range where the optical depth is 0.5. Festou and Atreya find $[CH_4] = 1.9^{+0.9}_{-0.3} \times 10^8$ cm^{-3} at an altitude of 966 km where $[H_2] = 1.2 \times 10^{12}$ cm^{-3}. At the same H_2 density, Smith et al. (1983) find the CH_4 density to be within a factor of 2 of Festou and Atreya's value.

The lightcurve, 1328–1412 Å (Fig. 3b) poses an unresolved dilemma.

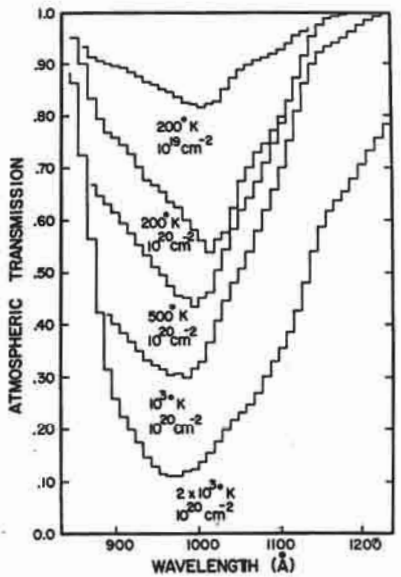

Fig. 4. Atmospheric transmission (as the Voyager 2 ultraviolet spectrometer would measure it) for isothermal lines of sight characterized by the indicated temperature and column densities (after Festou et al. 1981).

The onset of absorption at higher levels than in Fig. 3a and absorption to deeper and deeper levels (when one examines individual channels in 1328–1412 Å range) are not representative of the usual Jovian hydrocarbons, CH_4, C_2H_2, C_2H_6, C_2H_4 or any combination thereof. Although one cannot readily reject high-altitude haze (West et al. 1983*a*) as the possible absorber, it is difficult to reconcile the fact that it is not required below 1328 Å, but is needed above this wavelength to account for the observations. So far, the absorber responsible for attenuation of the flux shown in Fig. 3b has not been identified.

The analysis of the H_2 continuum absorption around 600 Å in the Voyager 2 solar occultation data at 29°5N yielded a temperature of 420 ± 30 K down to ~ 1600 km (Smith et al. 1983). The H Lyman-α analysis gives a thermospheric/exospheric temperature of 600^{+250}_{-150} K (G. R. Smith, personal communication, 1982). The temperatures in the homopause region deduced by Smith et al. from the stellar occultation data are in statistical agreement with those found by Festou and Atreya (1982). Unlike Festou and Atreya (1982), the stellar occultation analysis of Smith et al. above the homopause is dependent on the exospheric temperature they deduce from their solar occultation data. Note that the analysis of Smith et al. (1983) includes the newly published Rydberg series bands of H_2 (Shemansky and Ajello 1983). This, however, has no significant effect on the δ Sco stellar occultation results of Festou and Atreya (1982) for the following reasons:

1. As shown by Smith et al. (1983), inclusion of the additional Rydberg bands affects the H_2 absorption characteristics below 900 Å, and that too with a high H_2 column abundance of 10^{19} cm^{-2}. The δ Sco analysis of Festou and Atreya (1982) is for wavelengths > 939 Å, and the line-of-sight H_2 column abundance does not exceed 4×10^{18} cm^{-2} in the region where the exospheric temperature is reached;
2. As shown by Shemansky and Ajello (1983), inclusion of the Rydberg bands does not change the shape of the H_2 band structure for $H_2 > 10^{16}$ cm^{-2}. An important caveat in the δ Sco stellar occultation analysis of Smith et al. (1983) is that they use a single wavelength range, 939–1041 Å. Festou and Atreya (1982) have demonstrated that a single wavelength range yields a combination of line-of-sight H_2 column abundance and the exospheric temperature.

Indeed all temperatures between 400 K and 1000 K give a satisfactory fit to the lightcurves in the exospheric region. To define the temperature uniquely, one must analyze at least an additional wavelength range, as was done by Festou and Atreya (1982). The single most disconcerting uncertainty in the solar occultation analysis arises from the nonuniformity of the extreme-ultraviolet distribution on the solar disk (Atreya et al. 1979*a*); large areas of the Sun have been found to be 2 to 3 times brighter (and variable) than the average extreme-ultraviolet intensity of the Sun. The Sun subtends ~ 150 km in Saturn's atmo-

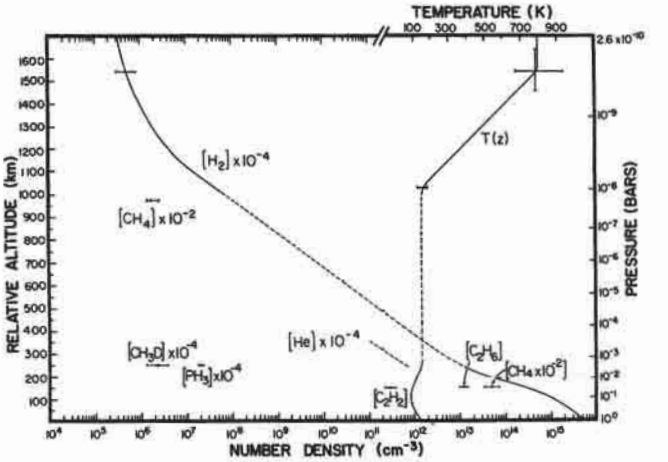

Fig. 5. Temperature and density profiles above the 1-bar atmospheric pressure level (after Festou and Atreya 1982). Atmospheric pressure corresponding to altitudes (left ordinate) is shown on the right ordinate. The interpolated regions of density and temperature at 250–950 km, are shown by broken lines. The helium density profile shown here is simply an illustration of its 6% volumetric mixing ratio in the homosphere. C_2H_2, C_2H_6, CH_4, CH_3D and PH_3 mixing ratios in the northern hemisphere are indicated by broken horizontal bars in the deep atmosphere, and taken from Courtin et al. (1982*a*).

sphere which is of the same order as the scale height for the 400 K exospheric temperature—further reducing the accuracy of the solar occultation analysis.

Until the discrepancy between exospheric temperatures derived from the solar occultation (Smith et al. 1983) and the stellar occultation (Festou and Atreya 1982) is satisfactorily resolved, it is reasonable to assume that there is a possibility of different exospheric temperatures at the 30° (solar occultation data), and the 4° (stellar occultation data) latitudes.

2. *Temperature and Density Profiles.* The distribution of temperature and densities in the upper atmosphere of Saturn derived by Festou and Atreya (1982) is shown in Fig. 5. The information above ~ 900 km is from the δ Sco stellar occultation experiment, while that in the lower stratosphere and troposphere is from Voyager infrared and radioscience experiments. There are no measurements in the middle atmosphere shown by a broken line interpolation in the temperature and H_2 density (10 nbar $\leq P \leq$ 1 mbar). The temperature at either end of this information gap is approximately 140 K (Festou and Atreya 1982; Hanel et al. 1981*a*; Tyler et al. 1981). From the hydrostatic equation, the average temperature of the information gap, 700 km, is 142 K. By

way of comparison, the information gap region on Jupiter is 275 km high with an average temperature of ~ 175 K. In terms of scale heights, the information gaps on the two planets are nearly equivalent: 11 to 12 scale heights high.

Studies of electron and ion energy loss processes indicate virtual equilibrium between plasma and neutral temperatures (Henry and McElroy 1969; Nagy et al. 1976; Waite 1981) at the heights of electron peaks. It is therefore instructive to compare the thermospheric neutral temperatures on Saturn with the plasma temperatures determined from the ionospheric scale height deduced by the Voyager radio occultation experiment: 565 K at 2800 km (ingress, 36°5N), and 617 K at 2500 km (egress, 31°S). The average low-to-midlatitude electron/ion temperature is then on the order of 600 K assuming that H^+ is the major topside ion. The error bars on the plasma scale height have not yet been published. An important caveat in the deduction of the plasma temperatures from the scale height data is that the determination of the average scale height is complicated by the presence of considerable structure in the ionosphere above the peak. Furthermore, the identity of the topside ion has not been determined. Note, however, that any ion other than H^+ would result in a greater temperature than the above-mentioned values.

Since the thermospheric energy budget is directly coupled to ionospheric processes, the discussion of the mechanisms for upper atmospheric heating is deferred to Sec. II.E, which follows the discussion of ionospheric calculations.

In addition to the upper atmospheric H_2 and CH_4 densities obtained from the δ Sco data, Fig. 5 also shows the homospheric densities of CH_4, C_2H_2, C_2H_6, CH_3D and PH_3 for the northern hemisphere (Courtin et al. 1982*a*), and the helium abundance (Hanel et al. 1981*a*) from the Voyager infrared measurements. The homospheric mixing ratios of the species are summarized in Table II. As evident in this table, there is a large latitudinal variation in the

TABLE II
Voyager Infrared Measurements of Mixing Ratios

Species	Mixing Ratio by Number ($[X_i]/[H_2]$) Northern Hemisphere[a]	Southern Hemisphere
CH_4	$1.85(+1.2, -0.5) \times 10^{-3}$	
C_2H_2	$1.2(+0.3, -0.3) \times 10^{-7}$	$0.5(\pm 0.1) \times 10^{-7}$
C_2H_6	$5.0(+1.1, -1.1) \times 10^{-6}$	$3.1(\pm 0.7) \times 10^{-6}$
CH_3D	$2.3(+1.5, -1.0) \times 10^{-7}$	
PH_3	$2.0(+0.3, -0.3) \times 10^{-6}$	
He	0.06	0.06

[a] The mixing ratios of C_2H_2 and C_2H_6 decrease sharply below the 20–50 mbar pressure level. The CH_4 mixing ratio may be as large as 5 times the solar, and there is a possible detection of Allene, $CH_2 = C = CH_2$ with an abundance of 0.3 cm atm (D. Gautier, personal communication, 1983).

mixing ratios of C_2H_2 and C_2H_6; abundances of the other hydrocarbons and PH_3 have not yet been determined for the southern hemisphere. The volume mixing ratio of helium at Saturn of 6% is approximately half this value at Jupiter. The depletion of helium in the upper atmosphere of Saturn is indicative of its probable condensation at the top of the metallic hydrogen zone, and the subsequent rain out of helium droplets toward the core of the planet (Ingersoll 1981).

B. Eddy Diffusion

In aeronomical problems, it is important to know the magnitude of vertical mixing or transport in a planetary atmosphere to determine the altitude distribution of minor species. Vertical mixing is generally expressed in terms of an all-encompassing parameter, the eddy diffusion coefficient K. At the homopause, the eddy diffusion coefficient is equal to the molecular diffusion coefficient. Beyond the homopause, diffusion processes are controlled by the molecular weights of individual species. Three methods have been used to determine the value of the eddy diffusion coefficient on Saturn: from the planetary Lyman-α albedo, from distribution of methane, and from He 584 Å airglow. We discuss below these techniques, their merits and deficiencies, and the results.

1. Lyman-α. Nonauroral Lyman-α emission from the outer planets is principally the result of resonance scattering of the solar Lyman-α photons by hydrogen atoms that lie above the methane homopause. Resonance scattering of interplanetary Lyman-α may contribute to the observed planetary emission for certain geometries. Hydrogen atoms below the homopause do not contribute appreciably to the Lyman-α albedo since methane is a strong absorber of the Lyman-α photons. Hunten (1969) adapted the terrestrial O-O_2 diffusion problem (Colegrove et al. 1965) to the atmosphere of Jupiter assuming a cold isothermal exosphere. Wallace and Hunten (1973) considered the problem of atomic hydrogen radiative transfer and chemistry by including previously neglected effects such as H production from CH_4 and some important scattering approximations. These calculations did not consider the possibility of high exospheric temperature and a gradient in the thermospheric temperature, since no clues to the Jovian upper atmospheric temperature were yet available. After the Voyager flyby of Jupiter, Waite (1981) considered these effects and also coupled the homosphere to the ionosphere where hydrogen atoms are produced either by photodissociation or dissociative photoionization of H_2. Once produced, the hydrogen atoms flow down to the deeper denser atmosphere where they are lost by 3-body recombination reactions.

The calculations of Waite (1981) for column abundance of hydrogen atoms as a function of the homopause eddy diffusion coefficient are shown in Fig. 6. These calculations are appropriate for the nonauroral region of Saturn with solar extreme ultraviolet alone responsible for the H production. Voy-

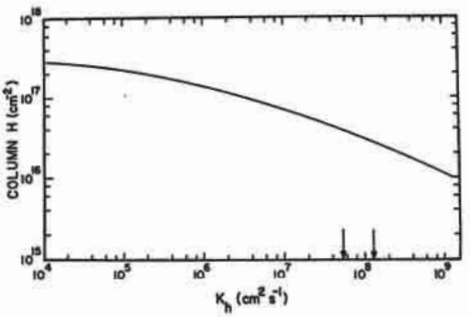

Fig. 6. Column abundance of atomic hydrogen above the unit optical depth level in methane as a function of the homopause value of the eddy mixing coefficient. These calculations assume the appropriate atmospheric temperature structure and the solar fluxes. The arrows represent the situations with and without the contributions of the interplanetary/interstellar Lyman-α backscattering to the observed planetary Lyman-α airglow. The corresponding values of K_h are 1.4 $\times$ 10^8 cm^2 s^{-1} and 8 $\times$ 10^7 cm^2 s^{-1}, respectively (adapted from Waite 1981).

ager's ultraviolet spectrometer measured between 3 and 3.3 kR of Lyman-α emission from the equatorial to midlatitude region (Broadfoot et al. 1981; Sandel et al. 1982*b*) implying atomic hydrogen column abundance of 4 $\times$ 10^{16} cm^{-2} above the level of the unit optical depth (τ) in methane. This value is uncertain to within a factor of 2 because of uncertainties in the solar Lyman-α flux. The observed planetary Lyman-α, however, is expected to include approximately 0.5 kR of the interplanetary/interstellar Lyman-α (Atreya 1982; Sandel et al. 1982*a*) so that only $\sim$ 2.5 kR could be attributed to the actual Saturnian Lyman-α. This latter value imples an H column abundance of approximately 2.7 $\times$ 10^{16} cm^{-2} above the τ = 1 level in methane. From Fig. 6, we find that the homopause eddy diffusion coefficients K_h corresponding to the above-mentioned hydrogen abundances are 8 $\times$ 10^7 cm^2 s^{-1} and 1.4 $\times$ 10^8 cm^2 s^{-1}, respectively. Sandel et al. (1982*b*) arrived at a similar value for K_h from their preliminary analysis of Saturn's Lyman-α albedo.

Sandel et al. (1982*a*) have also been able to reproduce the observed Lyman-α intensity with a value of 5 $\times$ 10^7 cm^2 s^{-1} for K_h and a simplified model for the hydrocarbon chemistry. They find that for a range of reasonable values of the solar Lyman-α flux at 1 AU of 6 $\times$ 10^{11} photons cm^{-2} s^{-1} (H. E. Hinteregger, personal communication, 1979) to 4 $\times$ 10^{11} photons cm^{-2} s^{-1} (Mount and Rottman 1981), the Saturn Lyman-α intensities obtained lie in the range 2.9 to 2.1 kR which are in reasonable agreement with the observations.

The major uncertainties associated with the above analysis, are: sources of H production other than the solar extreme ultraviolet, and the solar flux at

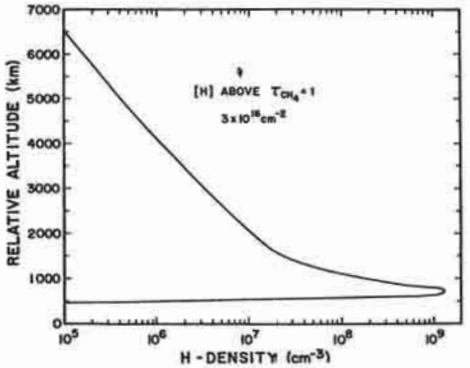

Fig. 7. Calculated atomic hydrogen density as a function of altitude for nonauroral region on Saturn (after Waite et al. 1983*a*).

Lyman α. Despite these complicating factors, we are confident that the above procedure of relating K_h to the Lyman-α emission rate is a reasonably good approximation. For example, calculations show (Fig. 7) that the solar extreme ultraviolet alone would produce approximately 3×10^{16} cm^{-2} hydrogen atoms above the $\tau = 1$ level in methane (Waite et al. 1983*a*) which is in good agreement with the above-mentioned value implied by the observed equatorial Lyman-α on Saturn. Thus, additional sources of H atoms are not required to explain the observations unlike on Jupiter at the time of the Voyager encounter.

Furthermore, the globally diluted downward flux of the H atoms produced in the narrow auroral region at Saturn (78–81° latitude, Sandel et al. [1982*b*]) is much smaller than that produced on the extreme-ultraviolet dissociation of H_2. For example, calculations by Waite et al. (1983*a*) yield an H atom flux of 5×10^8 cm^{-2} s^{-1} due to the extreme ultraviolet, while the flux resulting from the deposition of 1 to 10 keV electrons of 0.67 erg cm^{-2} s^{-1} energy is 3×10^{10} cm^{-2} s^{-1}. Although thermospheric winds on Saturn would tend to distribute globally the H atoms produced in the aurora, their contribution to the H flux due to the extreme-ultraviolet dissociation of H_2 would be negligible.

The Saturn Lyman-α emission has been monitored since 1977 and it appears to be more or less correlated with the variation in the solar Lyman-α flux or the solar extreme ultraviolet (Atreya et al. 1982*a*). One can, therefore, in principle exploit these data to determine the temporal variation in the upper atmospheric mixing. The pre-Voyager observations of the Lyman-α emission,

however, were carried out from Earth orbit, thus introducing ambiguities in the actual planetary Lyman-α emission due to the absorption of the Lyman-α photons in the interplanetary medium, and the possible contribution from the auroral Lyman-α.

2. *Methane.* The most direct method of determining the homopause level in an H_2 atmosphere is by monitoring the distribution of a heavier gas, such as methane whose density drops rapidly in the vicinity of the homopause. By comparing the measured CH_4 profiles with profiles calculated by varying K, one can determine the eddy diffusion coefficient. Again, one assumes that the CH_4 distribution is not affected by charged particle precipitation. The δ Sco ultraviolet stellar occultation experiment on Voyager 2 determined CH_4 density in the upper atmosphere (Festou and Atreya 1982). Assuming a reasonable variation of the eddy diffusion coefficient with the atmospheric number density M, such as $K \propto M^{-1/2}$ (which was found to be valid for Jupiter [Atreya et al. 1981]), and by varying K, Atreya (1982) calculated numerous theoretical models for the distribution of methane with photochemical and transport processes included. Shown in Fig. 8 are the H_2 densities at the altitude of unit vertical optical depth in methane at Lyman-α ($\tau^{\uparrow}_{CH_4} = 1$) vs. eddy diffusion coefficient at the homopause K_h. The $\tau^{\uparrow}_{CH_4} = 1$ level is found to be at an altitude of 800 km where the H_2 density is 1.6×10^{13} cm^{-3} (Festou and Atreya 1982). This implies K_h of 1.7×10^8 cm^2 s^{-1}, indicated by an arrow in Fig. 8. The altitude of the $\tau^{\uparrow}_{CH_4} = 1$ level, however, is uncertain so

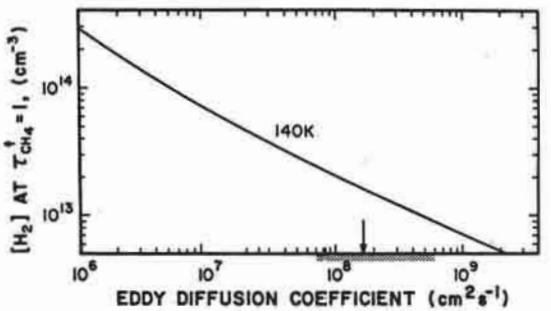

Fig. 8. H_2 density at the altitude of unit vertical optical depth in methane at Lyman-α vs. eddy diffusion coefficient at the homopause, K_h. The arrow represents the value of K_h corresponding to the central value of the H_2 density at the $\tau^{\uparrow}_{CH_4} = 1$ level determined from the δ Sco occultation data. The shaded area on the X axis corresponds to statistical uncertainty in the determination of the $\tau^{\uparrow}_{CH_4} = 1$ altitude level in the data (after Atreya 1982).

that the range of H_2 density at this level is between 9×10^{12} cm^{-3} and 2.5×10^{13} cm^{-3}; this would imply (from Fig. 8):

$$6 \times 10^8 \leq K_h \leq 7 \times 10^7 \text{ cm}^2 \text{ s}^{-1}. \quad (4)$$

This range for K_h is shown by the hatched area on the abscissa of Fig. 8. The homopause for CH_4 is determined to be at an altitude of 1110 km where the H_2 density is 1.2×10^{11} cm^{-3} and an atmospheric temperature of 250 K (Atreya 1982). Note that the $\tau^{\uparrow}_{CH_4} = 1$ level lies somewhat below the homopause, as was the case also for Jupiter (Atreya et al. 1981) due to the photolysis of methane.

3. He 584 Å. In a model developed for Jupiter, McConnell et al. (1981) have shown that analysis of the He 584 Å airglow data can yield information on the relationship between the eddy diffusion coefficient K_h at the homopause and the temperature structure. As K_h is increased, more He is transported into the upper atmosphere; the result is more scattering of the solar 584 Å line. As the temperature is increased, the relative amounts of He above the base of the scattering layer decreases by the change in the molecular diffusion coefficient with temperature. The results for Saturn, taken from Sandel et al. (1982*a*), are shown in Fig. 9. These results use the Voyager infrared interferometer spectrometer (IRIS) mixing ratio of 0.06 for helium (Hanel et al. 1981*a*).

Broadfoot et al. (1981) presented the first He 584 Å airglow data for the Voyager 1 encounter with Saturn. Since then the effects of the Jovian radiation belts on the calibration of the instrument have been better characterized (Holberg et al. 1982*a*); currently the best estimates of the He 584 Å intensity at the center of the disk are 3.1 ± 0.4 and 4.2 ± 0.5 R for Voyager 1 and Voyager 2 encounters, respectively. Since the solar flux at 584 Å does not appear to have changed (Sandel et al. 1982*a*), the implication of the change in the intensity is that either the temperature of the scattering region has changed by a factor of 2 or else, more likely, K_h has increased by a factor of 2. With the CH_4 homopause around 1110 km (Sec. I.B.2), the temperature in the scattering region is close to 250 K (Fig. 5) implying $7 \times 10^7 < K_h < 10^8$ cm^2 s^{-1} for the range of eddy coefficient (Fig. 9). The He homopause could, however, be located at a different altitude than the CH_4 homopause implying a somewhat different range of K_h.

Sandel et al. (1982*a*) have analyzed the δ Sco occultation data for the hydrocarbons in a different manner than Atreya (1982) to arrive at K_h; they have further attempted to relate it to the He 584 Å data discussed in Sec. I.B.4. The δ Sco occultation data used in this analysis refer to the 1160–1263 Å range (Fig. 10). The method adopts a lower atmosphere CH_4 mixing ratio of 1.6×10^{-3}. For an isothermal atmosphere, the distribution of CH_4 in the vicinity of the homopause is closely approximated by the formulae of Wallace and Hunten (1973). Referred to the homopause as the reference altitude, the

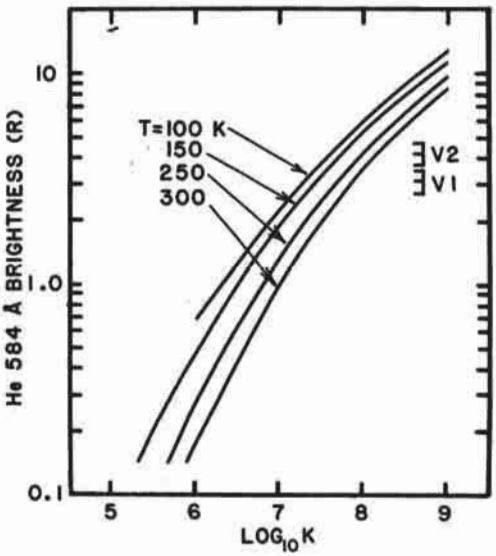

Fig. 9. He 584 Å airglow emission expected from Saturn as a function of the eddy diffusion coefficient at the homopause and the temperature in the scattering region. The brightnesses measured by Voyagers 1 and 2 are shown with their uncertainties on the right (after Sandel et al. 1982*a*).

shape of the CH_4 mixing ratio is invariant versus K in a density scale height frame. However, the attenuation offered to a solar beam is very sensitive to K (cf. Fig. 10). Fitting the data to the isothermal model the variation of K required to fit the data versus temperature can be obtained (Sandel et al. 1982*a*). This is illustrated in Fig. 11 which also shows the variation of K with T for the Voyager 2 He 584 Å airglow data. As can be seen, the CH_4 and He data are complementary, from which a unique value of K and T may be obtained. The results that Sandel et al. (1982*a*) obtained are given below.

$$T = 125^{+40}_{-25}\ \mathrm{K} \tag{5}$$

$$4 \times 10^7 < K_h < 1.2 \times 10^8\ \mathrm{cm^2\ s^{-1}}. \tag{6}$$

The range of values for K_h obtained in this manner is in reasonable agreement with those obtained by Atreya (1982) (see Sec. 1.B.2), in spite of the differences in analysis. From their recent solar and stellar occultation data, Smith et

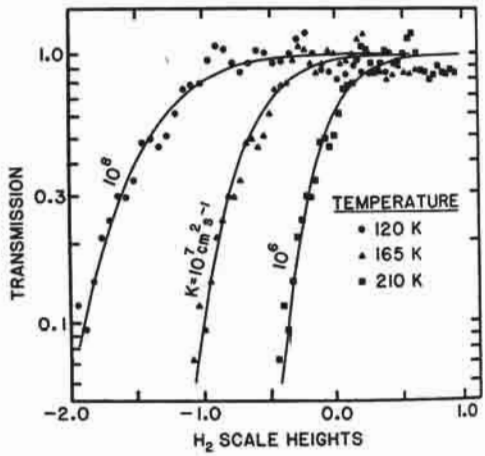

Fig. 10. Atmospheric transmission near Saturn's homopause vs. altitude. The unit of the abscissa is the H_2 scale height. The data points, which have been 1-2-1 smoothed, show the transmission measured in the 1160 to 1263 Å range plotted at scales corresponding to three temperatures. The solid curves are the transmission expected for CH_4 density distributions corresponding to the indicated eddy diffusion coefficients K. The three pairs of curves and data points represent pairs of T and K that are compatible with the measured CH_4 density distributions (after Sandel et al. 1982*b*).

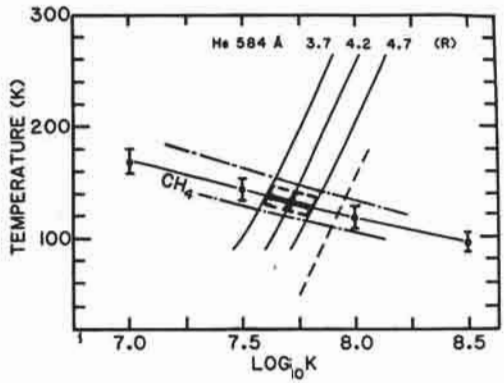

Fig. 11. Plots of the pairs of T and K satisfying the constraints imposed by the He 584 Å airglow brightness and measurements of the CH_4 density distribution. The two curves intersect at the unique pair that satisfies both sets of data and hence represents the conditions that hold near Saturn's homopause. The stippled area shows the uncertainty in T and K corresponding to the uncertainty in the two observations (after Sandel et al. 1982*b*).

al. (1983) derive $K_h = 5 \times 10^6$ cm^2 s^{-1}. This value is unacceptable since Smith et al. did not carry out a complete photochemical and transport modeling including coupling to the ionosphere, as done by Atreya et al. (1981) and Atreya (1982).

4. Comparison of K_h with Other Planets. Table III presents the best current values for the homopause values of eddy diffusion coefficients on Saturn, Jupiter, Titan, Earth, Mars and Venus. These values are pertinent to solar maximum conditions.

It is evident from Table III that during the Voyager encounters, the eddy coefficient on Saturn was greater than that on Jupiter or Earth at corresponding atmospheric densities. Such a difference could be the result of a different thermal structure in the middle atmosphere (D. M. Hunten, personal communication, 1982), or a more vigorous tropospheric dynamics on Saturn, perhaps driven by helium condensation (Atreya 1982). In any event, the Saturn measurements refer to a single point at one altitude and as such may not be representative for extrapolation to the lower atmosphere. There does not appear to be an appreciable difference between the homopause values of K_h on Saturn from the equatorial to the midlatitudes, as is evident from the results obtained from the δ Sco (equatorial) and the He 584 Å and Lyman-α (low to midlatitudes) analyses.

II. IONOSPHERE

Measurements of the ionospheric structure of Saturn were made by the Pioneer Saturn and Voyagers 1 and 2 spacecraft using the technique of radio occultation discussed in Sec. II.A. The measurements are reviewed in Sec. II.B. Theoretical models of the Saturn ionosphere are essentially similar to those of Jupiter. A review of the models is presented in Sec. II.C, while attempts to interpret these measurements with models are discussed in Sec. II.D. Finally, mechanisms of the thermospheric heating are discussed in Sec. II.E.

A. Ionospheric Measurement Technique

The structures of the ionospheres and tropospheres of the major planets have been successfully measured by the technique of radio occultation employed on both the Pioneer and Voyager spacecraft. Information on the gaseous envelope is obtained from measurements of Doppler frequency shift, group delay, intensity and polarization of the radio signal when the spacecraft swings behind the planetary body and undergoes occultation as viewed from the Earth (Eshleman 1973; Fjeldbo 1973; Hunten and Veverka 1976). The Pioneer measurements were carried out using a single frequency (2.293 GHz or S-band at 13 cm) while Voyager employed dual frequency (S-band, and X-band at 3.5 cm) radio links. The Voyager dual-frequency technique is particu-

TABLE III
Eddy Diffusion Coefficient

	K_h ($cm^2\ s^{-1}$)	Density[a] at Homopause (cm^{-3})	Altitude[b] of Homopause (km)	Atmospheric Pressure at Homopause (bar)	References
Saturn	$1.7(+4.3, -1.0) \times 10^8$ $8.0(+4.0, -4.0) \times 10^7$	1.2×10^{11}	1110	4×10^{-9}	Atreya (1982). Sandel et al. (1982*a*).
Jupiter	$1.4(+0.8, -0.7) \times 10^6$	1.4×10^{13}	440	10^{-6}	Atreya et al. (1981); McConnell et al. (1982*a*).
Titan	$1.0(+2.0, -0.7) \times 10^8$	2.7×10^{10}	3500	6×10^{-10}	E. J. Smith et al. (1982).
Earth	10^6	10^{13}	100	3×10^{-7}	Hunten (1975).
Venus	10^7	7.5×10^{11}	130–135	2×10^{-8}	Von Zahn et al. (1980).
Mars	$(1.3–4.4) \times 10^8$	$\sim 10^{10}$	135	2×10^{-10}	Nier and McElroy (1977).

[a] Density: H_2 for Jupiter and Saturn; atmospheric for others. Densities at the homopause correspond to the central values of K_h.
[b] Altitude: For Jupiter and Saturn, the altitudes are above the 1-bar atmospheric pressure level in the equatorial region; some previous publications had the cloud tops or the 10^{19} cm^{-3} level as the reference. For Titan, Earth, Venus and Mars, the altitudes are above the surface.

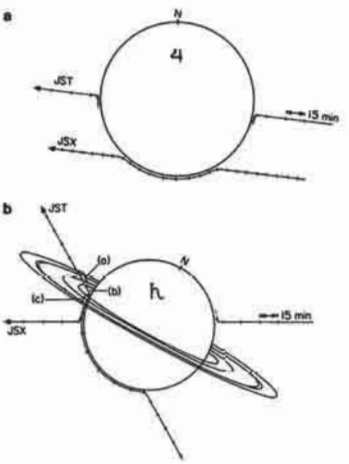

Fig. 12. *Upper diagram*: View from Earth of Voyager occultation at Saturn. The spacecraft radio images follow the indicated paths for the Jupiter-Saturn-Titan (JST) and Jupiter-Saturn-Uranus (JSX) trajectories. Note that there is a combination of near central and more grazing occultations. For JST at Saturn, region (a) provides a clear occultation of the rings and (b) a clear atmospheric occultation, while (c) is a combined ring and atmospheric occultation (after Eshleman et al. 1977). *Lower diagram*: Side view of Voyager occultations at Saturn. The trajectories are plotted in a rotating plane that instantaneously contains the Earth, the spacecraft, and the center of the planet. The pre-encounter values of latitudes of occultation immersions and emersions are shown, and regions (a), (b), and (c) of the upper view are also illustrated here (after Eshleman et al. 1977).

larly important for the Jovian and Saturnian ionospheres where multi-mode propagation of the beam is caused by sharp ionospheric layers (Eshleman et al. 1977). Furthermore, the signal-to-noise ratio for Voyager exceeds the Pioneer S-band values by 10 dB at S-band frequencies, and 23 dB at X-band frequencies (Eshleman et al. 1977). The occultation geometries at Saturn for the nominal Voyager Jupiter-Saturn-Titan (JST) and Jupiter-Saturn-Uranus (JSX) trajectories as viewed from the Earth are shown in Fig. 12. The latitudes of observations shown in the lower diagram of Fig. 12 are pre-encounter values, the actual latitudes, listed in Table II, are somewhat different.

B. Ionospheric Characteristics

The ionosphere of Saturn was probed on six occasions between 1979 and 1981. With the exception of the Voyager 1 exit data which have not been fully analyzed, major characteristics of all other measurements are listed in Table

TABLE IV
Ionosphere Observations of Saturn

Observation Date	Technique	Latitude	Solar Zenith Angle	Peak Electron Concentration (cm^{-3})	Altitude[a] of the peak above 1-bar level (km)	Plasma Scale Heights (km)
1979	Pioneer Saturn[b]					
Sept. 1	S-band					
	Ingress	11°.6S	89°.2 Terminator	1.1×10^4	1900	?[b]
	Egress	9°.7S	90°.9 Terminator	$\sim 1 \times 10^4$	2900	
1980	Voyager 1					
Nov. 12	S- and X-bands					
	Ingress	73°S	89° Late afternoon	2.3×10^4	2500	560 km
1981	Voyager 2					
Aug. 26	S- and X-bands					
	Ingress	36°N	87° Late afternoon	6.4×10^3	2850	1000 km, topside 260 km, lower
	Egress	31°S	93° Pre-dawn	1.7×10^4	2150	1100 km, topside

[a] 1-bar level is ~ 75 km below the level at which the atmospheric density of 10^{19} cm^{-3} is reached, and 50 km below the ammonia cloud tops.
[b] Although the plasma scale height cannot be determined with certainty in the Pioneer Saturn radio occultation data, the ingress data are more reliable. The data for $N_e < 3 \times 10^3$ cm^{-3} in these observations may be spurious.

IV. All measurements were made close to the terminator, i.e., at solar zenith angle $\approx 90°$.

The Pioneer radio occultation measurements revealed an ionosphere extending up to 30,000 km from the planetary limb (Kliore et al. 1980*a*). The entry (ingress) data are more reliable than the exit data. Data for concentrations < 3000 electrons cm^{-3} may not be indicative of the local electron concentration on Saturn; they are more likely due to electron fluctuations of the interplanetary solar wind (Kliore et al. 1980*b*). Fig. 13 shows the entry and exit ionospheric data up to a radius of 70,000 km. Despite differences in details, the two profiles show the same general characteristics. A peak electron concentration of $\sim 10^4$ cm^{-3} at ~ 1800 km occurs in the entry profile, while a similar peak concentration is found nearly 1000 km higher in the exit data. The magnitude of the electron fluctuations of the interplanetary solar wind associated with uncertainties in the orbit, and the oscillator drift render the exit data only marginally useful, and then only for qualitative comparison with the entry data (Kliore et al. 1980*a*). Due to insufficient information about the topside, it is also not possible to deduce a unique plasma scale height from these data. It is, however, apparent that the plasma temperature in the 63,000 to 68,000 km range is at least 500 K, and perhaps as high as 1000 K.

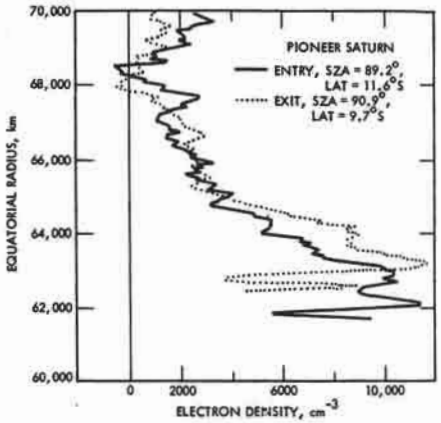

Fig. 13. Electron concentration in the ionosphere of Saturn between equatorial radii of 60,000 and 70,000 km. Solid curve is a profile produced from the closed-loop data taken during entry. The dashed curve is a profile obtained from exit data by using an artificial drift function and should be used only for comparison of features and not for magnitude of electron concentration (after Kliore et al. 1980*b*).

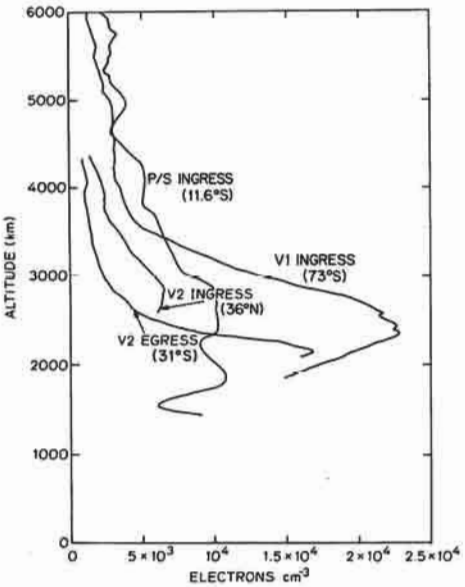

Fig. 14. Voyager 1 ingress, Voyager 2 ingress and egress, and Pioneer Saturn ingress ionospheric data plotted on a common altitude scale, the zero of which is at the 1-bar pressure level. The Voyager plots were prepared by L. Tyler and V. Eshleman on behalf of the Radio Science Team.

The Voyager 1 and 2 ionospheric measurements are shown in Fig. 14. For comparison, the Pioneer Saturn immersion data have also been plotted in this figure on the same scale as the Voyager data. The radio occultation experiment of Voyager 1 covered a latitude range from 73°S to 79°5S over a 14° range of longitudes (Tyler et al. 1981). The immersion ionospheric measurements were carried out very near the beginning of this exercise; the latitude of the ionospheric region probed was 73°S. A local peak at 2.4×10^4 cm^{-3} in the electron concentration was measured around 2500 km; above and below the peak, the electron profile appears to drop off rapidly. The topside plasma scale height of 560 km appears to be much smaller than that deduced from the Pioneer Saturn data. In either situation, it is difficult to determine the true plasma temperature from the scale height since the identity of the topside ion is not known with certainty (Sec. II.D). One can make only a qualitative comparison between the Pioneer Saturn and the Voyager data because of the

different observing frequencies and technique, and the fluctuations in the interplanetary solar wind electrons and the oscillator drift problems in the former. Furthermore, Voyager 1 data are particularly unsuitable for comparison as they represent polar conditions while the Pioneer data are for the equatorial region. The Voyager data analysis in the region below 2000 km is incomplete, and a considerably more complex structure is expected there (Tyler et al. 1982*a*) due, perhaps, to the presence of short-lived hydrocarbon ions and long-lived metallic ions as proposed for Jupiter (Atreya et al. 1974; Atreya and Donahue 1976). The metallic ions could be extraplanetary in origin such as from meteorites.

The Voyager 2 ionospheric measurements are for nearly midlatitude conditions, with immersion at 36°5N and emersion at 31°S (egress). Both measurements are made near the terminator, and both have peak electron concentrations somewhat lower than those measured on Voyager 1 in the polar region. The apparent peaks in the two Voyager 2 measurements are separated by nearly 700 km. The immersion data below 2500 km have not yet been analyzed, thus it is not entirely evident whether the observed peak is the main peak or simply a local maximum in the electron concentration profile. The topside scale height in the 2800–4000 km region of the ingress data is 1000 km, approximately twice the topside scale height for Voyager 1. The Voyager 2 egress ionospheric profile has approximately the same topside scale height (~1100 km) as the ingress one; the scale height just above the peak (2150 km) in the egress, however, is 260 km. Since the ionospheric data below ~ 2000 km have not been analyzed, it is suspected but not known whether the Saturn lower ionosphere would exhibit the type of multilayered structure seen on Jupiter.

C. Review of Theoretical Models

McElroy's (1973) review paper on the ionospheres of the major planets was the first theoretical attempt at modeling the Saturn ionosphere. He considered a neutral atmosphere composed of predominantly H_2, with He/H_2 and CH_4/H_2 ratios by volume of 0.3 and 10^{-3}, respectively. Earlier work by Gross and Rasool (1964) and Hunten (1969) had shown that in Jupiter's atmosphere every photon absorbed by H_2 leads to the production of two hydrogen atoms, either directly by

$$H_2 + h\nu \rightarrow H + H \tag{7}$$

or indirectly by

$$H_2 + h\nu \rightarrow H_2^+ + e^- \tag{8}$$

followed by

$$H_2^+ + H_2 \rightarrow H_3^+ + H \quad (9)$$

$$H_3^+ + e^- \rightarrow H_2 + H\,. \quad (10)$$

Since the atomic hydrogen produced by such processes could only be lost by 3-body recombination processes deep within the atmosphere, it was necessary to solve a diffusion equation to obtain the atomic hydrogen distribution. Knowledge of the H density distribution was required, since atomic hydrogen was the major source for the long-lived H^+ ions, the dominant ion species in past theoretical models of the Jovian ionosphere (Rishbeth 1959; Zabriskie 1960; Gross and Rasool 1964; Hunten 1969; Shimizu 1971). However, McElroy pointed out that all of the earlier studies had ignored the potential importance of dissociative ionization of H_2 as a source of H^+ ions. Following McElroy's suggestion, Atreya et al. (1974) included the above dissociative ionization process in their model of the Jovian ionosphere; it turned out to be the major source of topside ionization.

A comprehensive study of the ionospheres of other outer planets, i.e. Saturn, Uranus and Neptune, was carried out by Atreya and Donahue (1975*a*) using the same model atmosphere as McElroy, but including several important new chemical reactions, such as the 3-body recombination of H^+ and a new rate for H_3^+ electron recombination. This model again neglected ion diffusion, as had McElroy's model, but the changes in the chemical-reaction scheme resulted in some significant changes in the ionospheric profile. Atreya and Donahue were also the first to suggest the interaction of the ring particles with the ionosphere. In a follow-up study of the Saturn ionosphere carried out by Atreya and Donahue (1975*b*), their model considered the effect that reactions of H^+, H_3^+ and He^+ with CH_4 have on the structure of the ionosphere following another suggestion of McElroy (1973). Moderate values for the eddy diffusion coefficient ($K = 2 \times 10^6$ cm^2 s^{-1}) resulted in a pronounced hydrocarbon ion ledge below the ionospheric peak.

Further modeling of the Saturn ionosphere was carried out by Capone et al. (1977). They argued that due to the expected relatively weak magnetic fields of the outer planets and the decrease in solar extreme-ultraviolet radiation with increasing heliocentric distance, an ionospheric model of the outer planets is fundamentally incomplete without inclusion of galactic cosmic-ray ionization. However, the peak produced in their model by galactic cosmic rays occurred so deep in the atmosphere (at $\sim$ 0.5- to 1-bar level) that it had no influence on the main ionosphere but simply produced a low-lying ionospheric ledge.

From the Jovian ionospheric measurements it was apparent that high exospheric temperatures (Kliore et al. 1974; Fjeldbo et al. 1976; Atreya and Donahue 1976; Eshleman et al. 1979) and a wide range of values for the eddy diffusion coefficient (Cochran and Barker 1979) were also quite possible in the Saturn atmosphere. Waite et al. (1979) constructed a model to study the effect of variation of the eddy diffusion coefficient and exospheric tempera-

ture on ionospheric structure. This model used the ionospheric chemical scheme of the Jovian ionosphere (Atreya and Donahue 1976), but included the diffusion of the major ion H^+. The results of the Waite et al. model showed that for a cold isothermal thermosphere, values of the eddy diffusion coefficient from 10^4 to 10^6 cm^2 s^{-1} resulted in an ionosphere composed of H^+ ions with a peak electron density of $\sim 10^5$ cm^{-3}. Large values of the eddy diffusion coefficient ($\sim 10^9$ cm^2 s^{-1}) resulted in a large abundance of CH_4 being present at the level of maximum H_2 ionization, leading to a peak electron density of 10^3 cm^{-3}. High exospheric temperatures moderated this response through increased separation of the solar extreme-ultraviolet ionization region from the strong chemical loss of H^+ and H_2^+ in the methane layer.

D. Comparison Between Theoretical Models and Measurements

Since 1979 Pioneer Saturn and Voyager have measured the ionospheric structure of Saturn, as discussed in Sec. II.E. A major discrepancy exists between the measurements and the model prediction. All previous models predicted peak electron densities on the order of 10^5 cm^{-3}. The measurements indicate peak electron densities of $\sim 10^4$ cm^{-3}. Possible explanations include: decreased solar insolation due to shielding of the solar extreme-ultraviolet radiation by the rings (Waite 1981); the existence of a Saturn equatorial anomaly (Kliore et al. 1980*b*); photochemical loss due to reactions with CH_4 or OH (Shimizu 1980); and removal of topside ion H^+ by vibrationally excited H_2 (Atreya et al. 1979*b*; Atreya and Waite 1981; Waite 1981). A self-consistent ionospheric model which considers the above-mentioned effects has been developed by Waite et al. (1983*a*); its major points are discussed below.

Atreya and Waite (1981) attempted an interpretation of the Voyager radio science data by extending the ionosphere model developed by Waite (1981). They discussed the loss of H^+ via vibrationally excited H_2 mentioned above and the effect of vertical drifts on the magnitude and location of the peak in ionization. This calculation, however, assumed a preliminary atmospheric model. With the analysis of δ Sco stellar occultation data (Sec. II) it has been possible to construct a model of the ionosphere (Waite et al. 1983*a*) based on a neutral atmosphere measured simultaneously at nearly the same latitudes as the ionosphere. A calculation of the H_2 vibrational temperatures has also been included in this model to study the loss of H^+ via vibrationally excited H_2. Below, the model is discussed briefly, followed immediately by a summary of the calculated results.

The theoretical model used in the calculations of Waite et al. (1983*a*) consists of (1) a model neutral atmosphere including the major neutral species (H_2, He, H, CH_4, C_2H_6, C_2H_2, C_2H_4, and CH_3); (2) an ionospheric model based on the ion chemistry of earlier Jovian ionospheric models by Atreya and Donahue (1976) using the latest available rate constant as listed in Waite (1981) and Atreya and Waite (1981); (3) a 2-stream electron transport code including both photoelectrons and precipitating electrons; and (4) an ion and

electron temperature model. All components of this theoretical model are coupled together to provide a self-consistent solution to the composition, structure, and temperature of the Saturn ionosphere. A detailed description of the numerical model can-be found in Waite (1981). For background on the conservation equations of concentration, momentum and energy governing the ionospheric physics, the reader is referred to Banks and Kockarts (1973).

The details of the thermal structure, eddy diffusion coefficient, and the hydrocarbon mixing ratios are discussed in Sec. II and Fig. 5. Both the Festou and Atreya (1982) and the Smith et al. (1983) model atmospheres were used in the ionospheric calculations. Solar ultraviolet fluxes appropriate for the Voyager observations were provided by H. E. Hinteregger (personal communication, 1981).

The important sources and sinks of ionization are listed in Table V, and significant chemical reactions schematized in Fig. 15. Following ionization of the major atmospheric species H_2, He and H by solar extreme-ultraviolet radiation or electron impact, the resulting ions charge exchange with the neutral species giving rise to the numerous intermediate ions such as H_2^+, CH^+, CH_2^+, etc. The eventual topside ion is H^+ or H_3^+; immediately below the peak it is H_3^+, and in the deep atmosphere several hydrocarbon ions such as CH_5^+, $C_2H_5^+$, $C_3H_8^+$, etc. are expected to be prevalent. The terminal ions in the various regions of the atmosphere are all lost by electron recombination. We discuss below the characteristics of the equatorial/midlatitude and auroral ionosphere calculations.

For the low and midlatitude regions, solar extreme-ultraviolet radiation provides the dominant source of ionization. Fig. 16 shows for the Festou and Atreya (1982) model atmosphere, a model of the ionosphere based on this ionization source (Waite et al. 1983*a*). There is considerable disagreement between the measurements and the calculations with regard to both the height and the magnitude of the ionospheric peak. The model calculations indicate a peak electron density of 2×10^5 cm^{-3} located 1200 km above the ammonia cloud tops whereas the measurements indicate peak densities of 1×10^4 cm^{-3} at altitudes between 2000 and 3000 km. A similar disagreement also resulted when the Smith et al. (1983) model atmosphere was used. In this case the peak electron density was 3.7×10^5 cm^{-3} and located at 1450 km. The scale height of the ionosphere was significantly less than that of the ionosphere model from the Festou and Atreya (1982) model atmosphere. For this model atmosphere, there is a rough agreement with the plasma scale heights from Voyager 2 measurements which indicate temperatures on the order of 600 to 1000 K, if we assume that $T_e = T_i$. This is a reasonable assumption since plasma temperatures remained in thermal equilibrium with the neutral temperature in the model calculations at altitudes below 4750 km due to strong H_2 vibrational cooling of the electrons.

Previous calculations have suggested that vertical drifts (Kliore et al. 1980*b*; Waite 1981; Atreya and Waite 1981; Atreya et al. 1982*b*; McConnell

TABLE V

Important Chemical Reactions in the Ionosphere of Saturn[a]

Reaction Number	Reaction	Rate Constant	References
Ion Production			
p1	$H_2 + h\nu \rightarrow H_2^+ + e$		
p2	$\rightarrow H^+ + H + e$		
p3	$H_2 + e \rightarrow H_2^+ + 2e$		
p4	$\rightarrow H^+ + H + 2e$		McElroy (1973).
p5	$H + h\nu \rightarrow H^+ + e$		
p6	$H + e \rightarrow H^+ + 2e$		
p7	$He + h\nu \rightarrow He^+ + e$		
p8	$He + e \rightarrow He^+ + 2e$		
p9	$CH_3 + h\nu \rightarrow CH_3^+ + e$		Atreya and Donahue (1975*b*).
Charge Exchange			
e1	$H_2^+ + H_2 \rightarrow H_3^+ + H$	2.0×10^{-9}	Theard and Huntress (1974).
e2	$H_2^+ + H \rightarrow H^+ + H_2$	6.4×10^{-10}	Karpus et al. (1979).
e3	$He^+ + H_2 \rightarrow H_2^+ + He$	$\leq 2.0 \times 10^{-14}$ (sum 1×10^{-13})	
e4	$\rightarrow HeH^+ + H$	$\leq 2.0 \times 10^{-14}$ (sum 1×10^{-13})	Johnsen and Biondi (1974).
e5	$\rightarrow H^+ + H + He$	$< 8.0 \times 10^{-14}$ (sum 1×10^{-13})	
e6	$He^+ + CH_4 \rightarrow CH^+ + H_2 + H + He$	2.4×10^{-10}	Huntress (1974).
e7	$\rightarrow CH_2^+ + H_2 + He$	9.3×10^{-10}	Huntress (1974).
e8	$\rightarrow CH_3^+ + H + He$	9.6×10^{-11}	Adams and Smith (1976).
e9	$\rightarrow CH_4^+ + He$	1.6×10^{-11}	Adams and Smith (1976).
e10	$H^+ + H_2 + H_2 \rightarrow H_3^+ + H_2$	2.2×10^{-29}	Miller et al. (1968).

TABLE V (continued)
Important Chemical Reactions in the Ionosphere of Saturn[a]

Reaction Number	Reaction	Rate Constant	References
e11	$H^+ + H_2(v' \geq 4) \rightarrow H_2^+ + H$	$k = fn(T_v)$	(see text)
e12	$H^+ + CH_4 \rightarrow CH_3^+ + H_2$	2.3×10^{-9}	Huntress (1974).
e13	$\rightarrow CH_4^+ + H$	1.5×10^{-9}	Huntress (1974).
e14	$HeH^+ + H_2 \rightarrow H_3^+ + He$	1.85×10^{-9}	Theard and Huntress (1974).
e15	$H_3^+ + CH_4 \rightarrow CH_5^+ + H_2$	2.4×10^{-9}	Huntress (1974).
e16	$CH^+ + H_2 \rightarrow CH_2^+ + H$	1.0×10^{-9}	Huntress (1974).
e17	$CH_2^+ + H_2 \rightarrow CH_3^+ + H$	1.6×10^{-9}	Smith and Adams (1977).
e18	$CH_3^+ + CH_4 \rightarrow C_2H_5^+ + H_2$	1.2×10^{-9}	Smith and Adams (1977).
e19	$CH_4^+ + CH_4 \rightarrow CH_5^+ + CH_3$	1.5×10^{-11}	Smith and Adams (1977).
e20	$CH_4^+ + H_2 \rightarrow CH_5^+ + H$	3.3×10^{-9}	Smith and Adams (1977).
Electron-Ion Recombination			
r1	$H_3^+ + e \rightarrow H_2 + H$	$2.8 \times 10^{-7} \left(\frac{200}{T_e}\right)^{0.7}$	Leu et al. (1973).
r2	$H_2^+ + e \rightarrow H + H$	$<1.0 \times 10^{-8}$	Auerbach et al. (1977).
r3	$HeH^+ + e \rightarrow He + H$	$\sim 1.0 \times 10^{-8}$	Hunten (1969).
r4	$H^+ + e \rightarrow H + h\nu$	$4.0 \times 10^{-12} \left(\frac{250}{T_e}\right)^{0.7}$	Bates and Dalgarno (1962).
r5	$He^+ + e \rightarrow He + h\nu$	$4.0 \times 10^{-12} \left(\frac{250}{T_e}\right)^{0.7}$	Bates and Dalgarno (1962).
r6	$CH_5^+ + e \rightarrow CH_4 + H$	3.9×10^{-6}	Maier and Fessenden (1975).
r7	$C_2H_5^+ + e \rightarrow C_2H_2 + H + H_2$	3.9×10^{-6}	Maier and Fessenden (1975).

[a]Table adapted from Atreya and Donahue 1976 and Atreya et al. 1979.

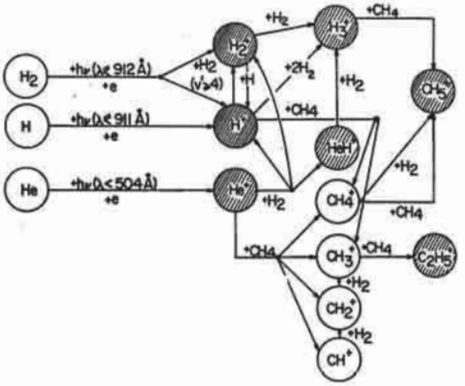

Fig. 15. Schematic of the Jovian and Saturnian ionospheric reactions (after Atreya and Donahue 1982).

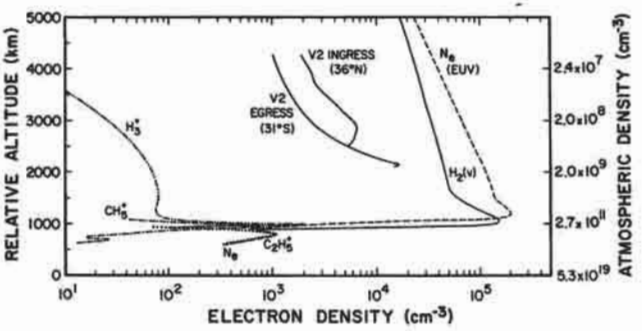

Fig. 16. Calculated ionospheric profiles for the nominal midlatitude model, curve N_e, and the Voyager data for the midlatitudes. The effect of vibrationally excited H_2 (by extreme ultraviolet) on the electron concentration is shown by the curve $H_2(v)$ (after Waite et al. 1983*a*).

et al. 1982*b*) and high H_2 vibrational temperatures (Atreya and Waite 1981) may be important in determining the height and magnitude of the ionospheric peak on Saturn. McConnell et al. (1982*a*) have also carried out calculations for Jupiter which show that reasonable theoretical fits to the ionospheric data can be obtained with appropriate choices for the vertical drift and H_2 vibrational temperature. The difficulty with previous calculations is the lack of jus-

tification for the somewhat arbitrary choice of the H_2 vibrational temperature profile and vertical drift rates needed to provide agreement between theory and measurement.

To quantify the uncertainty, Waite et al. (1983*a*) have carried out H_2 vibrational level calculations for the Saturn upper atmosphere for midlatitudes using in these calculations the Festou and Atreya (1982) model atmosphere. At an altitude of 1200 km, where the calculated electron density is at a maximum, the vibrational temperature T_{vib} for the fourth level is about a factor 3 larger than the neutral temperature. For a reaction rate for $H^+ + H_2$ ($v' \geq 4$) of 2×10^{-9} cm^3 s^{-1}, this degree of vibrational excitation is sufficient to reduce the calculated electron density from 2.3×10^5 cm^{-3} to 1.5×10^5 cm^{-3} (see the profile for H_2(v) in Fig. 16). At an altitude of 2500 km, where the observed electron density is $\sim 10^4$ cm^{-3}, T_{vib} ($v' = 4$) is twice the neutral temperature and reaction of H^+ with H_2(vib) is the dominant sink of H^+. The calculated N_e is now 4×10^4 cm^{-3}, in better agreement with the radio occultation results (see Fig. 16).

Model calculations were also carried out for the auroral ionosphere (Waite et al. 1983*a*). The neutral atmosphere was taken from Festou and Atreya (1982), with the exception that the altitude scale is now somewhat compressed due to the larger gravity at higher latitudes. The effects of precipitating electrons were included using the 2-stream electron transport code (Waite 1981; Waite et al. 1983*b*). Monoenergetic electrons at 1 and 10 keV with a total energy flux of 0.67 ergs cm^{-2} s^{-1} were introduced at the top of the model atmosphere (6500 km). The total calculated Lyman and Werner band emission intensity was 7.1 kR in the 10 keV case and 6.4 kR for the 1 keV case, which is close to the observed average intensity of the auroral emission (Broadfoot et al. 1981; Sandel et al. 1982*b*). The peak emission altitude in the 10 keV case was only 1 to 2 scale heights above the level of unit optical depth of CH_4 ($\tau^{\uparrow}_{CH_4} = 1$ level) but the emission for 1 keV was well above the $\tau^{\uparrow}_{CH_4} = 1$ level. Precipitating auroral electrons most probably lie within this range of energies since Voyager 2 measurements by the ultraviolet spectrometer show little hydrocarbon extinction of the Lyman and Werner bands but some self-absorption (Sandel et al. 1982*b*). The resulting ionospheric profiles (Waite et al. 1983*a*) are shown in Fig. 17. The nominal 1 keV case (marked 0 K) indicates a peak electron density of 4×10^6 cm^{-3} at 1200 km, whereas the nominal 10 keV case indicates a peak density of only 3×10^5 cm^{-3}. The difference is due to the different atmospheric levels at which auroral energy is deposited. For the 1 keV electrons, the maximum electron impact ionization rate is at 1050 km (near the level of extreme-ultraviolet H^+ production peak at 950 km); for the 10 keV electrons it is at 750 km, which is well within the region of strong proton loss via reaction with methane.

At high latitudes where the auroral precipitation dominates, the 1 keV and 10 keV electron precipitation generates very large amounts of vibrationally excited H_2. However, there are two other factors which tend to mod-

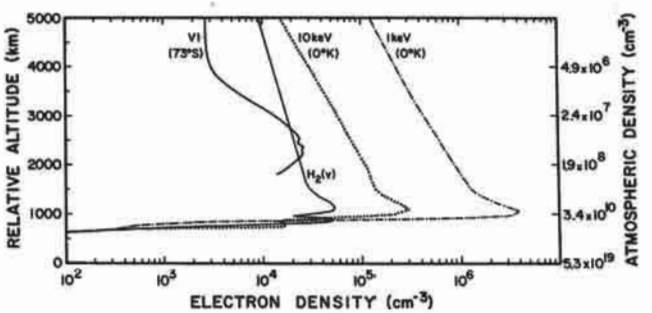

Fig. 17. Calculated ionospheric profiles in the auroral zone of Saturn for the 1-keV and 10-keV electron beams (dot-dashed and dotted lines, respectively). The Voyager 1 measurement for the high latitudes is marked V1 (73°S). The effect of the H_2 vibrational distribution on the ionospheric H^+ is also shown by the curve marked $H_2(v)$ for the 1 keV case (after Waite et al. 1983*a*).

erate the ionospheric effects of the large vibrational production rates. In the first place, the electron precipitation also produces copious amounts of H^+, so that any vibrationally excited H_2 must work harder to remove it. Second, there is also a large production rate of H resulting in H densities almost a factor of 100 larger than at midlatitudes—if this atomic hydrogen is not redistributed to lower latitudes by thermospheric winds. Large H densities tend to keep the lid on T_{vib} because vibrationally excited H_2 is readily quenched by H. The high-latitude electron density observed at 2250 km can be reproduced by the reaction of H^+ with H_2 ($v' \geq 4$) (see the $H_2(v)$ profile, the 1 keV auroral case in Fig. 17), if the H density at auroral latitudes is reduced near the midlatitude values by thermospheric redistribution (Waite et al. 1983*a*).

In conclusion, calculations indicate that vibrationally excited H_2 probably plays a major role in controlling the ionosphere of Saturn. It provides the most likely explanation, though not the only one, for the discrepancy between the observed electron densities and the ones calculated using the nominal ionospheric model with vibrationally excited H_2. However, several outstanding problems must be resolved in order to further quantify the effects of vibrationally excited H_2 on H^+ in the Saturn ionosphere. First and foremost, the reaction rate for the proposed $H^+ + H_2$ ($v' \geq 4$) reaction must be measured in the laboratory. Furthermore, a realistic evaluation of the effects of vertical drifts and vibrationally hot H_2 on the concentrations would require the knowledge of electron profiles at low altitudes.

Other potential possibilities for reconciling the observed ionospheric structure and the calculations include loss of the major ion H^+ on reaction

with CH_4 or OH. Waite (1981) has found that for eddy diffusion coefficients less than a few times 10^9 cm^2 s^{-1}, the loss due to reaction with CH_4 is not important because CH_4 is not mixed to high enough altitudes unless the ionosphere undergoes strong diurnal vertical drifts that move the peak below the methane homopause. Such a scenario might help explain the apparent diurnal variations of the peak electron density from 100 cm^{-3} to 2×10^5 cm^{-3} as inferred from Saturn's electrostatic discharges (Kaiser et al. 1983; chapter by Kaiser et al.). Significant diurnal variations of electron density could then be explained in terms of the height of the ionospheric peak with respect to the methane layer. Shimizu (1980) has argued for a loss mechanism involving reaction of H^+ with the hydroxyl radical OH. Indeed, the source of OH may be in the rings of Saturn, as is evident from the laboratory experiments of W. L. Brown et al. (1982) on the energetic charged particle erosion of water ice. Although it is potentially an important loss mechanism for H^+, in order to explain the observed electron concentrations, an unreasonably large concentration of the OH radicals (on the order of 10^4 to 10^5 cm^{-3}) is required throughout the entire altitude range. Perhaps a way could be found to arrive at large OH fluxes into Saturn's atmosphere, without affecting the stability of the rings. One could conceive of other extraplanetary sources of water, such as meteorites or the icy satellites of Saturn.

E. Thermospheric Heat Sources

Several potential heat sources may play a role in determining the thermal structure in the upper atmosphere of Saturn. They include photoelectrons, gravity waves, energetic electron precipitation, and Joule heating; each source is discussed below.

1. Solar Extreme-Ultraviolet Heating. The calculations by Strobel and Smith (1973) estimated a small (10 K) rise in the temperature of the upper atmosphere of Jupiter as a result of solar extreme-ultraviolet heating. The major heating mechanism is chemical heating due to the formation of H_2^+ and subsequent reactions which result in the recombination of H_3^+. The overall process releases 10.95 eV of heat per H_2 ionization. The second most important source of extreme-ultraviolet heating is photoelectron impact dissociation of H_2 followed by a host of lesser sources such as indirect and direct vibrational excitation of H_2 (Cravens 1974).

The total column-integrated extreme-ultraviolet heat source in the upper atmosphere is only 3×10^{-3} erg cm^{-2} s^{-1} (Waite 1981), a factor of 100 smaller than that required to reproduce the exospheric temperature measured by Voyager 2 (Festou and Atreya 1982). The heating rate of column-integrated thermal electrons from photoelectrons is only 6×10^{-4} erg cm^{-2} s^{-1} and is insufficient to raise the electron temperature above the neutral temperature at any altitude in the ionosphere.

2. Inertia-Gravity Waves. The breaking of inertia-gravity waves as a source of heat in the upper atmosphere of the major planets was first suggested by the stellar occultation measurements of Jupiter (Veverka et al. 1974). This mechanism could produce a temperature profile similar to the inferred profile, if breaking of inertia-gravity waves 4 to 6 scale heights above the methane homopause was capable of depositing ~ 0.3 erg cm^{-2} s^{-1}. Although the dissipation of this much energy is consistent with the 3.4 erg cm^{-2} s^{-1} that French and Gierasch (1974) estimated to be available from the inertia-gravity waves propagating upward in the Jovian ionosphere, the magnitude of the inertia-gravity wave source for Saturn cannot be determined until a classical tidal calculation is carried out. Furthermore, it is not apparent if the waves would dissipate and deposit heat (and if so, at what height) or would simply be reflected.

3. Electron Precipitation. Electron precipitation is also a possible heat source, as discussed in the context of Jupiter by Hunten and Dessler (1977). Recent Voyager ultraviolet spectrometer measurements of Saturn's airglow estimate an average auroral electron energy influx of 2×10^{11} W between 78° and 81°.5 latitude in both the northern and southern hemispheres (Sandel et al. 1982*b*). Model calculations of the ultraviolet spectrum from $e + H_2$ excitation by Shemansky and Ajello (1983) indicate that the energy of the electrons responsible for the auroral Lyman and Werner band emission is between 1 and 10 keV and that the Saturnian auroral spectrum can be produced solely by direct products of the $e + H_2$ process.

The altitude of peak heating is also a function of the precipitating electron energy. More energetic electrons deposit their energy at greater atmospheric densities. The altitude separation between the heat source and the infrared cooling level (i.e., the hydrocarbon level) determines the exospheric temperature for a thermosphere where vertical conduction is the dominant heat transfer process. Therefore, 1 keV electrons result in higher exospheric temperatures for a given column heating value than 10 keV electrons because the effects of increased heating efficiencies at higher electron energies are more than offset by the effect of the smaller altitude separation between the heat source and sink. The same is true for soft electrons below 100 eV which deposit their energy near the 10^8 cm^{-3} density level.

A one-dimensional heat conduction equation was solved for both a 10 keV and 1 keV electron aurora with a total energy flux of 0.67 erg cm^{-2} s^{-1}. Similar calculations were done for Jupiter by Hunten and Dessler (1977). The 1 keV electrons generate an exospheric temperature of ~ 1600 K at 1500 km, and the 10 keV electrons produce an exospheric temperature of ~ 650 K at 900 km on Saturn. Auroral deposition would appear to be an important source of high-latitude heating in Saturn's thermosphere. However, even if the entire auroral energy of 2×10^{11} W were distributed with a 100% efficiency over the entire planet, it would amount to < 0.01 erg cm^{-2} s^{-1}, which is inade-

quate for raising the low-latitude thermospheric temperature over the homopause value by any appreciable degree. It should be noted that in the case of Jupiter energetic oxygen and sulfur ions (10–30 MeV/nuc) can supply 10^{13} to 10^{14} W into the auroral region (Gehrels and Stone 1983). However, no such energetic heavy ions diffusing inward to Saturn have been identified.

Electron precipitation can also produce heating of the thermal electron population. However, electrons with energies between 1 and 10 keV with a total energy flux of up to 10 erg cm^{-2} s^{-1} produce no departure from thermal equilibrium at altitudes where the neutral density is $> 10^7$ cm^{-3} (Waite 1981). Soft electrons (< 100 eV) which deposit sufficient energy above the 10^8 cm^{-3} atmospheric density level can, however, cause substantial departures of the plasma temperature from the neutral temperature. Small electron precipitation energy fluxes of the order of 0.25 erg cm^{-2} s^{-1} can result in electron temperatures on the order of 5000 to 10,000 K in the topside ionosphere with accompanying order of magnitude increases in the electron density at altitudes from 2000 to 3000 km (Waite et al. 1983*b*). The eventual fate of this electron heating is to be conducted down to the 10^7–10^8 cm^{-3} atmospheric density level where it cools to the neutral atmosphere.

4. Joule Heating. Joule heating arises from the presence of electric currents in the ionosphere. In its most rudimentary form, the Joule heating rate for the neutral gas is given by

$$J = \sigma_p E^2 \tag{11}$$

where σ_p is Pedersen conductivity (Banks and Kockarts 1973) and E is electric field. Joule heating has been shown to be a major source of thermospheric heating on Earth. A study by Heaps (1976) of the Jovian atmosphere indicated that Joule heating was not expected to be an important heat source for that planet. However, Heaps underestimated the electric fields. Atmospheric electric field values extrapolated from the measured departure of the magnetospheric plasma from planetary corotation (McNutt et al. 1979) produce Joule heating rates of 5 erg cm^{-2} s^{-1} in the Jovian thermosphere at high latitudes (Waite 1981). In fact, detailed Joule heating calculations by Nishida and Watanabe (1981) indicate heating rates > 10 erg cm^{-2} s^{-1} in the high-latitude ionosphere of Jupiter.

McNutt (1983*a*) has suggested that there is a significant (10%) departure of the Saturn magnetosphere from planetary corotation in the outer magnetosphere. We can estimate the implied Joule heating rate at 80° latitude in the Saturn ionosphere using the method of Nishida and Watanabe (1981). The height-integrated Pedersen conductivity at these latitudes is 58 mhos according to a calculation by Waite et al. (1983*a*) (Fig. 18). Therefore, a 10% departure of the magnetosphere from the planetary rotation rate will result in a Joule heating rate of 0.14 erg cm^{-2} s^{-1}. This rate is comparable to the heating

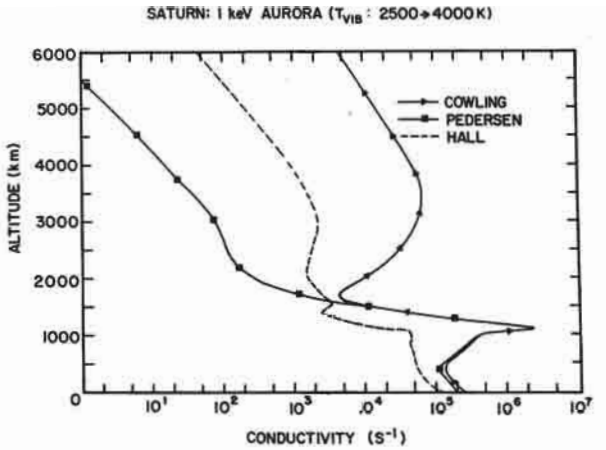

Fig. 18. Calculated conductivity profiles for the 1-keV ionospheric calculation shown in Fig. 17. The height integrated conductivities are: 75.4 mhos (by Cowling); 58.0 mhos (by Pedersen); and 9.1 mhos (by Hall). By way of comparison, the height-integrated Pedersen conductivity in the auroral region on Jupiter is calculated by Strobel and Atreya (1983) to be ~ 10 mhos.

rates inferred for the auroral zone, ~ 0.3 erg cm^{-2} s^{-1}, from the measured H_2 Lyman and Werner band emissions. It should be emphasized, however, that the above-mentioned Joule heating rate is the upper limit since it is based on a model ionosphere which gives electron concentrations far too high in comparison with the measurements. Once the lower ionospheric data have been analyzed, it may turn out that the model electron concentrations are still higher than the data. Until all the data have been analyzed, and a good model fit obtained, Joule heating for Saturn remains of potential value. Possible interaction of the plasmasphere with the rings may be a significant additional source of Joule heating for the high- and low-latitude thermosphere (Waite 1981).

III. SUMMARY AND FUTURE PROSPECTS

A self-consistent picture of the thermal structure, composition, vertical mixing, ionospheric distribution, and energy budget of the upper atmosphere of Saturn has begun to emerge from the recent Voyager measurements of the neutral and plasma environments of Saturn. It is found that the average temperature in the middle atmosphere is approximately 140 K, thus not drastically different from that in the corresponding region on Jupiter. The ex-

osphere of Saturn, at 600–800 K, however, is considerably cooler than the Jovian exosphere where temperatures on the order of 1100 K were recorded at about the same epoch and latitude. Unlike Jupiter, however, auroral particle precipitation does not directly supply sufficient energy for the observed thermospheric/exospheric heating on Saturn, and it also does not contribute significantly to the global distribution of the hydrogen atoms. Joule heating appears to be a promising candidate for accounting for the observed exospheric temperature on Saturn. The vertical mixing at the Saturn homopause is found to be about a factor of 100 greater than the value at the Jovian homopause, again around the same period. Greater eddy mixing on Saturn could result from a possible different stratospheric/mesospheric thermal structure, or the turbulence associated with proposed separation from hydrogen and rain out of helium toward the core. A discrepancy between the observed electron density profiles and the models can be resolved provided that large H_2 vibrational temperatures and the ion vertical drifts are present. Despite major new advances in the upper atmospheric physics and chemistry of Saturn made from the interpretation of Voyager observations, further breakthroughs will require understanding of the dynamics, seasonal effects, thermochemistry, and evolution of Saturn about which relatively little is now known, either theoretically or observationally. Following is a brief list of specific issues which need further investigation:

1. Additional analysis of the Voyager ultraviolet spectrometer data in the wavelength region 1100–1700 Å is required to determine the height profiles of C_2H_2 and C_2H_6. This is a particularly difficult problem since it involves absorption by a mixture in which the proportions of individual components are rapidly changing with height. The identity of the absorbers in the 1328–1412 Å range needs to be established. A possible candidate is H_2O (from an extraplanetary source of O, OH, or H_2O), but one must beware of its low vapor pressure at the relevant temperatures in Saturn's atmosphere. Once the height profiles of the hydrocarbons and other species have been obtained, photochemical models should be calculated for comparison, and for studying the validity of the chemical schemes.
2. Resolution of the discrepancy between the exospheric temperatures obtained from the solar occultation at 30° and the stellar occultation at 4° requires additional work. To fully understand the stellar occultation data, the calculations of Smith et al. (1983) should be extended to include the variation of temperature in the line of sight, absorption at $[H_2] > 10^{21}$ cm^{-2} (line-of-sight column), and additional sets of wavelength ranges in which H_2 absorption occurs. Some of these calculations necessitate the use of large computers.
3. Since the Voyager measurements generally refer to a given location on Saturn, the global distributions and seasonal variations can be only modeled from considerations of thermospheric and mesospheric dynamics.

Data for upper atmospheric dynamics are lacking; future spacecraft missions should ensure inclusion of instruments for dynamics measurements.

4. No satisfactory heat source has yet been proposed for Saturn's thermosphere. Both Joule heating and the inertia-gravity wave mechanisms need further investigation.
5. The modeling of ionospheric structure and the resulting conductivities require a thorough analysis of the radio occultation data below ~ 2000 km.
6. Laboratory rate-constant measurements for the reaction between H^+ and the vibrationally excited H_2 must be carried out to understand its role in Saturn's topside ion chemistry.

Acknowledgment. We thank D. M. Hunten and an anonymous referee for valuable suggestions. We acknowledge individually or jointly useful conversations with V. Eshleman, M. Festou, J. Holberg, B. Sandel, D. Shemansky, G. Smith, D. Strobel, and L. Tyler. This work was supported by NASA Planetary Atmospheres Program, NASA Voyager Contract, and by the Natural Sciences and Engineering Research Council of Canada.